Beatriz Pelaz[1#], Pablo del Pino[2#], Pauline Maffre[3#], Raimo Hartmann[1], Marta Gallego[2], Sara Rivera-Fernández[4], Jesus M. de la Fuente[5], G. Ulrich Nienhaus[3,6*], Wolfgang J. Parak[1,2*]

[1] Fachbereich Physik, Philipps Universität Marburg, Marburg, Germany
[2] CIC biomaGUNE, San Sebastian, Spain
[3] Institute of Applied Physics and Institute of Toxicology and Genetics, Karlsruhe Institute of Technology (KIT), Karlsruhe, Germany
[4] Instituto de Nanociencia de Aragon, University of Zaragoza. Zaragoza, Spain
[5] Instituto de Ciencia de Materiales de Aragon, CSIC/University of Zaragoza, Zaragoza, Spain
[6] Department of Physics, University of Illinois at Urbana-Champaign, Urbana, IL, USA
[#] these authors contributed equally to this work
[*] corresponding authors: uli@uiuc.edu; wolfgang.parak@physik.uni-marburg.de

Surface functionalization of nanoparticles with polyethylene glycol (PEG): Effects on human serum albumin adsorption and cellular uptake

Abstract:

Here we have investigated the effect of enshrouding polymer-coated nanoparticles (NPs) with polyethylene glycol (PEG) on the adsorption of proteins and uptake by cultured cells. PEG was covalently linked to the polymer surface to the maximal grafting density achievable under our experimental conditions. Changes in the effective hydrodynamic radius of the NPs upon adsorption of human serum albumin (HSA) were measured *in situ* by using fluorescence correlation spectroscopy (FCS). For NPs without a PEG shell, a thickness increase of around 3 nm, corresponding to HSA monolayer adsorption, was measured at high HSA concentration. Only 50% of this value was found for NPs with PEGylated surfaces. While the size increase reveals formation of a protein corona also for PEGylated NPs, fluorescence lifetime measurements and quenching experiments suggest that the adsorbed HSA molecules are buried within the PEG shell. *In vitro* uptake of the NPs by 3T3 fibroblasts was reduced to around 10% upon PEGylation with PEG chains of 10 kDa. Thus, even though the PEG coatings did not completely prevent protein adsorption, the PEGylated NPs still displayed a pronounced reduction of cellular uptake with respect to bare NPs, which is to be expected if the adsorbed proteins are not exposed on the NP surface.

Introduction:

Colloidal nanoparticles (NPs) come into contact with the biological environment *via* their surfaces. Thus, for biomedical applications, NPs surfaces need to be carefully designed to elicit the desired effect, such as targeting to specific epitopes. By contrast, other applications may demand that NPs are not recognized by their environment, *e.g.*, to avoid their clearance by the immune system. To endow NPs with such "stealth" properties, modification of their surfaces with polyethylene glycol (PEG) has become a popular method. It reduces NP uptake by cultured cells *in vitro*[1-7] and by entire organisms *in vivo*, so that retention times of NPs in the blood circulation are increased[8-13]. These effects are often "explained" by postulating that PEGylation prevents formation of a protein corona and, thus, NPs are not recognized by the immune system. Indeed, there is experimental evidence supporting a reduced tendency of proteins to adsorb onto PEGylated surfaces, *e.g.*, by using mass spectrometry or gel electrophoresis[5,14-16]. In general, dense PEG coatings, which can vary with respect to the molecular weight and grafting density of the polymer, reduce the adsorption of opsonins *in vivo*. The formation of an opsonin corona would immediately alert the phagocyte system,[17] thereby promoting rapid clearance of the NP-opsonins complex from the blood stream. Likewise, PEGylation of NPs has been used traditionally *in vitro* to reduce unspecific interactions with serum proteins, which typically results in a reduced uptake by cultured cells compared with uptake of their non-PEGylated counterparts. That said, the formation of a protein corona can also hinder the interaction of NP ligands with the cellular membrane, resulting in a reduced uptake[18].

The problem of protein adsorption onto PEGylated surfaces has attracted enormous attention of many researchers in the context of planar surfaces[19-25]. It has become clear that protein adsorption strongly depends on the density of PEGylation as well as on the molecular weight of the PEG chains employed[5,20,22,26]. The highest grafting density of PEG on surfaces can be obtained by growing PEG chains from monomers *in situ*, thereby ensuring a tight surface coverage[14,27,28]. Such layers are very efficient in preventing protein adsorption, especially, when growing long PEG chains. If PEG polymers are covalently attached to a surface[14,29,30], the grafting density is limited by the PEG chain entropy, which drives PEG into a random coil shape, thereby hindering a close spacing of anchoring groups on the surface[27,31]. Proteins may penetrate less dense PEG layers, reside in voids[32], and even approach and interact with the underlying reactive surfaces. Accordingly, an efficient strategy to prevent protein penetration into PEG layers has been to use star-shaped PEGs with reactive ends that allow dense crosslinking of the PEG surface layer[33-35]. Densely grafted, planar PEGylated surfaces have been reported to completely suppress protein adsorption, but only in certain configurations[31,36,37].

These findings are also of great relevance for studies of protein adsorption onto the spherical surfaces of PEGylated NPs. Most often, NPs are PEGylated by covalently binding entire PEG chains to NP surfaces, which limits the grafting density to values below those achieved by *in situ* growth. For such cases, it was shown that surface-bound PEG chains are coiled rather than stretched, resulting in a packing density below the theoretical maximum[38,39]. In addition, the curvature of the NP surface also has an effect on the density of surface ligands, as has been discussed in detail for the linkage of oligonucleotides to NP surfaces[40,41]. Thus, protein adsorption resistance of NPs can vary greatly, depending on the PEGylation strategy employed. However, even with reduced polymer surface density and, thus, presumably less than optimal protein-repellent coating, PEGylated NPs have shown markedly increased *in vivo* blood circulation retention times[10] as well as reduced *in vitro* NP uptake by cells[42,43].

The protein-repellent nature of the NP surface is not the only effect of PEGylation. Other important physicochemical parameters of the NPs are likewise affected[44]. Most obvious is a change in size, as measured by the hydrodynamic radius[39]. Indeed, a NP size increase above a certain threshold, ~ 50 nm in the case of citric acid stabilized Au NPs, has been reported to reduce NP incorporation by cultured cells[45]. PEGylation can also modify the surface charge of NPs, even if nominally uncharged PEG molecules (*e.g.*, with a terminal hydroxy or methoxy group) are used. This effect may result from a reduction of the number of charged groups on the NP surface, if they are in part utilized as anchoring points for PEG linkage, but also due to chelation of cations by the PEG chains[38]. Such a reduction in surface charge may affect colloidal stability. Often, NPs are stabilized in solution by electrostatic repulsion, and they may lose colloidal stability due to charge screening by counter ions at physiological salt concentrations (ionic strength around 150 mM)[46]. PEGylation, however, confers colloidal stability to NPs *via* steric repulsion, even under high salt conditions. Increase in colloidal stability has been linked to a decrease in NP uptake by cells *in vitro*[42]. To summarize, besides changes in surface chemistry PEGylation of a NP has three distinct additional effects: (1) It increases its size and (2) its colloidal stability, and (3) it may reduce its surface charge density. All three effects typically lead to less efficient incorporation by cells[47]. Therefore, to better understand the effect of PEGylation on nano-bio interactions of NPs, it is important to disentangle the effect of reduced protein adsorption from its direct effects on the physicochemical properties of the NPs.

In this study, we have quantitatively investigated protein adsorption on well characterized PEGylated and non-PEGylated NPs. These NPs have an inorganic core and are coated with a shell of an amphiphilic polymer with integrated fluorophores, making them colloidally highly stable and, at the same time, endowing them with bright fluorescence emission[48]. The polymer-coated NPs can be conveniently

PEGylated by linking PEG chains to the NPs surface, resulting in a coiled PEG geometry[38,39]. They show reduced uptake by cells *in vitro* [42] as well as enhanced blood circulation retention times *in vivo* [10]. We have previously quantified protein adsorption onto similar NPs (without PEG) *in situ*[49-51], employing fluorescence correlation spectroscopy (FCS)[52]. In these model studies, we had dissolved the NPs in buffer solutions in which individual protein species such as serum albumin or transferrin were present in well-defined concentrations varying over several orders of magnitude. Towards higher protein concentrations, monolayers of proteins were observed to adsorb onto the NPs. The strength of the NP-protein interaction could be characterized by the midpoint of the binding transition, *i.e.*, an apparent dissociation coefficient, K_D'. In the present work, these techniques are applied to PEGylated NPs.

Experimental Procedures:

FePt NPs, with a radius, r_c = 1.6 ± 0.2 nm, of the inorganic core, were coated with an amphiphilic polymer based on poly(maleic anhydride-*alt*-dodecene) (PMA) labeled with the fluorescent dye DY-636 according to published protocols[49] (for details, we refer to Supporting Information). This polymer renders the NPs water soluble by carboxyl groups exposed on the NP surface. The solution containing the polymer-coated NPs was purified from residual polymeric micelles by gel electrophoresis[53]. PEG chains of different molecular weight (M_W = 750 Da, 5 kDa, 10 kDa) were linked to the NP surfaces *via* standard bioconjugate chemistry (*i.e., via* amide-bond formation between terminal amino groups on the PEG chains and the carboxyl groups of the polymer) to the maximum extent possible, as confirmed by gel electrophoresis[38]. Negative TEM staining was used to determine the core-shell radius r_{cs} of the PEGylated NPs. We also prepared PMA-coated Fe_3O_4 NPs with a larger inorganic core, r_c = 4.0 ± 0.6 nm, but without PEGylation as a control sample of NPs with different size. Furthermore, we prepared PMA-coated FePt NPs surface-modified with glucose as a control sample of NPs with a reduced surface charge.

All NPs were thoroughly characterized using transmission electron microscopy (TEM), inductively coupled plasma mass spectrometry (ICP-MS), UV/Vis absorption and fluorescence spectroscopy, gel electrophoresis, dynamic light scattering (DLS), fluorescence correlation spectroscopy (FCS), and laser Doppler anemometry (LDA). The adsorption of human serum albumin (HSA) on the surface of the different NPs was quantitatively analyzed *in situ* by using FCS, yielding a precise determination of the hydrodynamic radius of the NPs with adsorbed proteins as a function of the HSA concentration, and a simple binding model allows us to compute the apparent dissociation coefficient K'_D, the maximum number of proteins N_{max} bound per NP, the corona thickness Δr_h, and the Hill coefficient n[49]. Note that similar studies have been

performed recently by others using DLS[54]. In addition, incorporation of the NPs by 3T3 cells was quantified *in vitro* by immunostaining and confocal microcopy[55].

Results and Discussion:

Schematic depictions of all NP samples used in this study are shown in Figure 1. The most important experimentally determined physicochemical parameters of the NPs are compiled in Table 1.

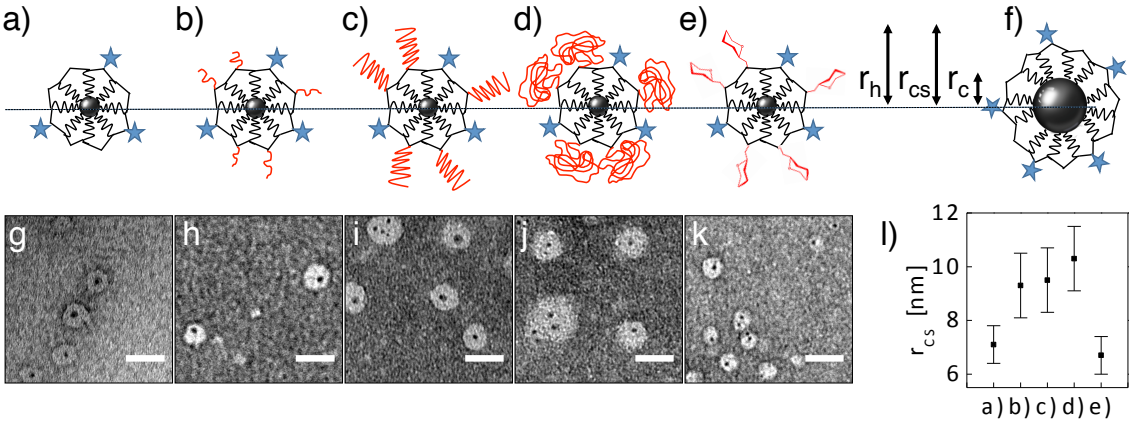

Figure 1: Sketch of the different NP samples studied in this work. All NPs contain an inorganic core with radius r_c, represented by a black sphere in the center. They are coated with the amphiphilic polymer PMA, to which the fluorophore DY-636 (drawn in light blue) was linked covalently [48]. PEG chains of different M_w or glucose (drawn in red) were linked to the NP surfaces, resulting in different hydrodynamic radii r_h. a) FePt-PMA, b) FePt-PMA-PEG750, c) FePt-PMA-PEG5k, d) FePt-PMA-PEG10k, e) FePt-PMA-glucose, f) Fe_3O_4-PMA. The lower panels show selected ROIs of negatively stained TEM micrographs (scale bar: 25 nm) for g) FePt-PMA, h) FePt-PMA-PEG750, i) FePt-PMA-PEG5k, j) FePt-PMA-PEG10k, and k) FePt-PMA-glucose. l) Comparison of the mean core-shell radius r_{CS} of the FePt samples, as determined by negative staining TEM analysis (data were derived from the images shown in Supporting Information, *cf.* Figures I.10-I.14).

Sample	a)	b)	c)	d)	e)	f)
NP core	FePt	FePt	FePt	FePt	FePt	Fe_3O_4
Shell composition on top of PMA layer	–	PEG (750 Da)	PEG (5 kDa)	PEG (10 kDa)	glucose	–
r_c [nm] (TEM)	1.6±0.2	1.6±0.2	1.6±0.2	1.6±0.2	1.6±0.2	4.0±0.6
r_{cs} [nm] (TEM)	7.1±0.7	9.3±1.2	9.5±1.2	10.3±1.2	6.7±0.7	-
r_h [nm] (DLS)	4.2±0.2	4.8±0.5	6.5±0.7	10.6±0.9	4.6±0.6	6.2±0.2
r_h [nm] (FCS)	5.4±0.1	6.5±0.1	7.9±0.2	9.7±0.2	5.4±0.1	6.7±0.2
ζ [mV]	–44±3	–17.8±0.5	–28±1	–14.3±0.4	–25±3	–55±3

Table 1: Physicochemical parameters of the different NPs consisting of inorganic core, PMA polymer and PEG/glucose shell, with inorganic core radii r_c (TEM) and geometric core/shell radii r_{cs} (TEM, negative staining), as determined in the dried state. The hydrodynamic radii r_h of the different NPs were measured in water with DLS (number distribution) and in phosphate buffered saline without divalent ions (PBS, pH = 7.4) with FCS (shown is the fit parameter $r_h(0)^{(fit)}$). Zeta potentials, ζ, were determined in water using LDA (number distribution). All raw data are included in the SI.

As expected, PEGylation leads to an increase in NP size (TEM (negative staining), DLS and FCS) and, concomitantly, to a reduction in the magnitude of surface charge (LDA), *i.e.*, they are less negatively charged. Considering that a single PEG monomeric unit is 44 Da in weight and 0.35 nm in length, the contour lengths of our PEG chains (*i.e.*, the length of PEG in hypothetically fully stretched conformation), with M_w of 750 Da, 5 kDa and 10 kDa amount to, respectively, 6 nm, 40 nm and 80 nm. However, the hydrodynamic radius increase upon PEGylation is only between 1 and 6 nm for the three different PEG chains. These results clearly indicate that the PEG chains are not stretched, but coil, fold or twist on the NP surface, in full agreement with previous reports[39]. In fact, the size increase with PEG weight rather scales with the radius of gyration of free PEG in its random coil conformation (*cf.* Supplementary Information for details)[39]. For FePt-PMA-glucose, no size increase was observed, but a reduction in surface charge, as for the PEGylated NPs. In contrast, NPs with bigger cores (Fe_3O_4 instead of FePt, *i.e.*, Fe_3O_4-PMA) had an increased hydrodynamic radius, but maintained a similar surface charge as those with smaller cores but without PEGylation. Thus, the two control samples, one with an increased hydrodynamic radius but similar surface charge (Fe_3O_4-PMA), and the other one with a reduced surface charge but similar hydrodynamic radius (FePt-PMA-glucose) enable us to separate effects specific for PEG surface functionalization from changes in basic physicochemical properties accompanying PEGylation, namely, changes in size and surface charge.

Colloidal stability of all NPs was probed by additional DLS studies. No significant size increase was found in NaCl solutions of different concentrations, demonstrating the high colloidal stability of all the NPs. Therefore, our NPs were well dispersed and did not show noticeable agglomeration tendency, in good agreement with previous data concerning the colloidal stability of PMA-coated NPs (*cf.* the Supporting Information for data)[56,57].

Due to the integrated fluorophores, FCS can be conveniently used to detect the diffusion of the NPs in the presence of proteins *in situ*, without any interference due to unbound proteins emitting background fluorescence[49,58-60]. The different NPs were incubated in PBS with varying concentrations of human serum albumin (HSA). At each

concentration *c*, the resulting hydrodynamic radius of the NPs with adsorbed proteins $r_h(c)$ was determined *via* FCS, using a previously reported confocal microscope[51]. The resulting $r_h(c)$ curves were fitted using a model based on the volume of the adsorbed proteins, the number of which is described by the Hill equation (see Supporting Information)[49,58], *cf.* Figure 2, leading to the following fit parameters for each type of NP: the hydrodynamic radius $r_h(0)$ of the NPs in the absence of proteins, the increase in hydrodynamic radius Δr_h upon saturating the NP surface with HSA, the Hill coefficient n, the maximum number N_{max} of HSA molecules bound per NP at saturation, and the apparent dissociation coefficient K'_d (*i.e.*, the free protein concentration at which $N_{max}/2$ HSA molecules are bound to the NP on average). The results are summarized in Table 2.

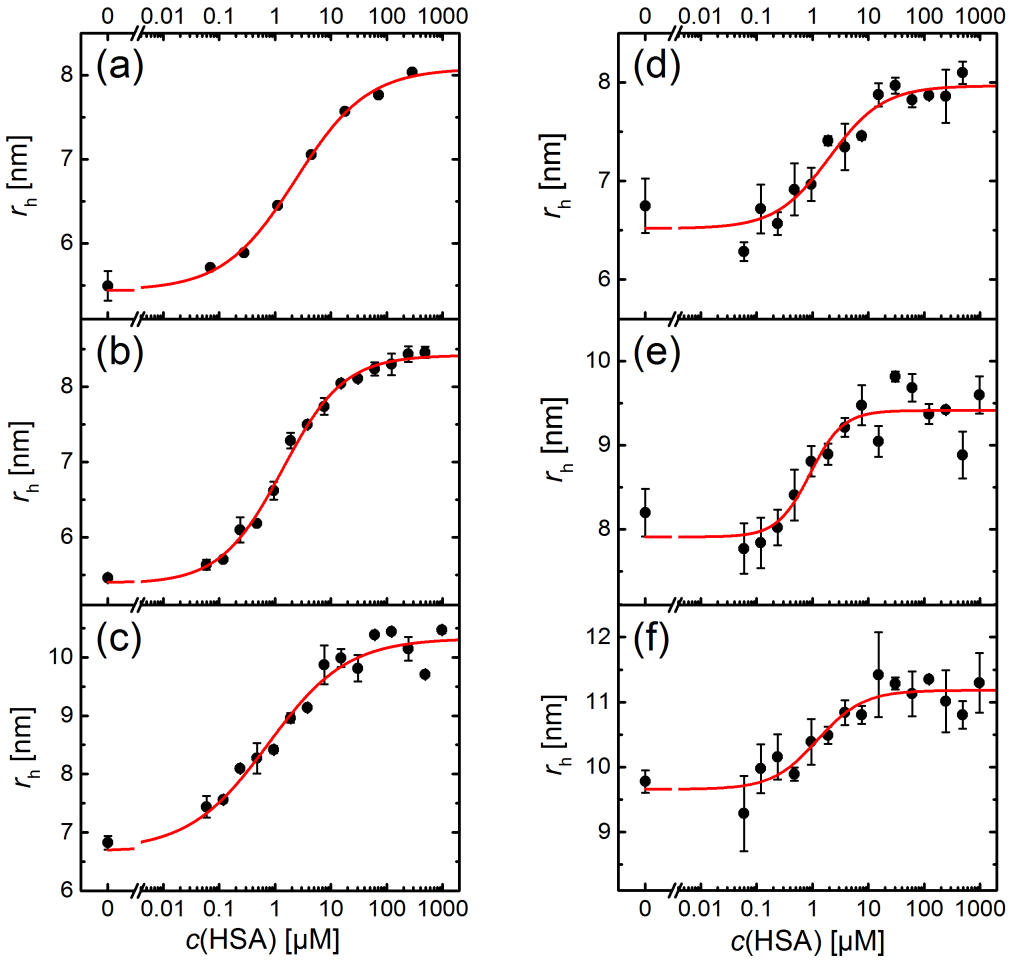

Figure 2: Hydrodynamic radius r_h as measured for the different NP species upon the presence of different concentrations *c* of HSA in PBS, and the corresponding fits based on the Hill model. (a) FePt-PMA, (b) FePt-PMA-glucose, (c) Fe_3O_4-PMA, (d) FePt-PMA-PEG750, (e) FePt-PMA-PEG5k, (f) FePt-PMA-PEG10k. The fit parameters are shown in Table 2.

NP core	FePt	FePt	FePt	FePt	FePt	Fe_3O_4
surface modification	-	PEG	PEG	PEG	glucose	-

		(750 Da)	(5 kDa)	(10 kDa)		
$r_h(0)$ [nm]	5.5±0.2	6.7±0.3	8.2±0.3	9.8 ± 0.2	5.5±0.1	6.8±0.2
$r_h(0)^{(fit)}$ [nm]	5.4±0.1	6.5±0.1	7.9±0.2	9.7 ± 0.2	5.4±0.1	6.7±0.4
Δr_h [nm]	2.6±0.1	1.4±0.2	1.5±0.3	1.5±0.3	3.0±0.1	3.6±0.5
$r_h(c_{max})^{(fit)}$ [nm]	8.1±0.1	7.9±0.1	9.4±0.2	11.2±0.2	8.4±0.1	10.3±0.3
K'_d [μM]	4.1±0.8	2.0±1.0	1.0±0.4	1.4±0.7	2.3±0.3	1.5±0.5
N_{max}	15.2±0.8	9.0±1.0	14.0±2.0	21.0±3.0	18.3±0.7	33.0±4.0
n	0.7±0.1	0.9±0.3	1.5±0.8	1.1±0.5	0.8±0.1	0.6±0.2
$N_{max} / 4\pi r_h^2(0)^{(fit)}$ [nm^{-2}]	0.041± 0.003	0.017± 0.002	0.018± 0.003	0.018± 0.003	0.050± 0.003	0.06± 0.01
$4\pi r_h^2(0)^{(fit)} / N_{max}$ [nm^2]	24±2	59±7	56±9	56±9	20±1	17±3

Table 2: Compilation of parameters as obtained from a least-squares fit of the protein adsorption model to the FCS data in Figure 2. $r_h(0)$ is the hydrodynamic radius of the NPs directly in PBS without HSA added. $r_h(0)^{(fit)}$ is the size of the NPs without HSA added, as obtained from fitting the measured $r_h(c)$ data points with the model described in Supporting Information. The fit also returns the parameters K'_d, N_{max}, Δr_h and n, which are the apparent dissociation coefficient, maximum number of proteins bound per NP, corona thickness, *i.e.*, the difference in radius of NPs saturated with proteins and NPs without proteins, and the Hill coefficient, respectively. $r_h(c_{max})^{(fit)} = r_h(0)^{(fit)} + \Delta r_h$ is the hydrodynamic diameter of the NPs saturated with HSA. $N_{max} / 4\pi r_h^2(0)^{(fit)}$ is the number of HSA proteins adsorbed onto a NP per unit of surface area, which is assumed to be $4\pi r_h^2(0)^{(fit)}$. The mean surface area occupied per bound protein is given in the last row (*i.e.*, the inverse of $N_{max} / 4\pi r_h^2(0)^{(fit)}$).

HSA adsorption onto the polymer-coated FePt NPs was found to be in good agreement with our previous reports, only the radius increase with increasing protein concentration for non-PEGylated FePt NPs was slightly smaller than in previous studies [49,51]. For all PEGylated NP preparations, the size likewise increased with increasing protein concentration, indicating that HSA associates with our PEGylated NPs. The binding affinity, which is inversely related to the apparent dissociation constant K'_d, was similar for PEGylated and non-PEGylated NPs (FePt-PMA-PEG *versus* FePt-PMA). The size increase due to HSA corona formation was only ~1.5 nm for the FePt-PMA-PEG NPs and thus reduced by roughly a factor of two from the values obtained for the non-PEGylated NPs (FePt-PMA, FePt-PMA-glucose, Fe_3O_4-PMA). This is a very interesting result because the obtained thickness, 1.5 nm, is less than the smallest extension of HSA (~3 nm). This finding may be explained in two different ways: Either fewer HSA proteins bind to PEGylated NPs than to non-PEGylated NPs, or a similar number of HSA proteins may be adsorbed, but they may partially penetrate into the

PEG layers of PEGylated NPs, resulting in repulsion of hydration water and, consequently, a denser coating layer than for FePt-PMA NPs. Both possibilities will be discussed below. Notably, the PEG chain length had no influence on the HSA binding affinity (K'_d) or the HSA corona thickness (Δr_h).

As pointed out in the introduction, modified protein adsorption upon PEGylation could simply arise from the size increase of the PEGylated NPs. For this reason, we studied bigger, PMA-coated NPs without PEGylation as a control. Because a well-controlled procedure to increase the core size of our FePt NPs was not available, we instead employed Fe_3O_4 NPs with a bigger core diameter, but with exactly the same PMA polymer coating. Considering that the inorganic cores (FePt, Fe_3O_4) are completely buried in the polymer shell, we can presume that both types of NPs are essentially identical with respect to their surface properties. This view is also supported by the ζ-potentials of both NPs (FePt-PMA, Fe_3O_4-PMA), which are identical within the experimental error (*cf.* Table 1). The data in Table 2 show that the size increase of the smaller FePt-PMA NPs and the bigger Fe_3O_4-PMA NPs upon saturation with HSA (Δr_h) are very similar, corresponding to a monolayer of HSA proteins. However, since the surface area of the Fe_3O_4-PMA NPs is greater than the one of the FePt-PMA NPs, the number of adsorbed HSA molecules per NP (N_{max}) is increased. Therefore, we have calculated the number of proteins per surface area (N_{max} / $4\pi r_h^2(0)^{(fit)}$), *cf.* Table 2. This number is identical for FePt-PMA and Fe_3O_4-PMA NPs. Thus, the size increase of PMA-coated NPs from $r_h(0)^{(fit)}$ = 5.4 nm to $r_h(0)^{(fit)}$ = 6.7 nm did not affect HSA protein adsorption. In contrast, when the surface chemistry was modified by PEGylation, a significant change in the interactions can be seen. The Fe_3O_4-PMA and FePt-PMA-PEG750 samples have essentially identical hydrodynamic radii $r_h(0)^{(fit)}$ and, thus, identical surface areas. This result clearly shows that the reduced thickness change due to HSA adsorption, Δr_h, upon PEGylation is directly correlated with the specific properties of the PEG shell, and not related to the accompanying change in NP size (within the size range investigated here).

The FePt-PMA-glucose NPs[16] showed comparable HSA adsorption properties as the FePt-PMA NPs, although their ζ-potential was reduced and more similar to the ζ-potentials measured for PEGylated NPs. Currently, neither the precise number of glucose molecules attached *per* NP nor their location and orientation on the surface is known. Certainly, the geometry of the glucose molecules on the NP surface is expected to play an important role. In fact, if they are partly buried in the polymer shell, a protein repellent effect may be absent. Despite this lack of knowledge about their surface structure, the FePt-PMA-glucose NPs serve here as an important control. Like the PEGylated NPs, they had a reduced surface charge. However, glucose modification did not change the hydrodynamic radius, and the same amount of HSA adsorbed onto FePt-PMA-glucose NPs as onto FePt-PMA NPs (in terms of N_{max} as well as N_{max} /

$4\pi r_h^2(0)^{(fit)}$). Thus, the change in protein adsorption that we have observed for the PEGylated samples does not result from a reduction in surface charge accompanying PEGylation, but has to be ascribed definitively to the intrinsic properties of the PEG layer.

The two control experiments demonstrate that there is a specific effect of PEG to reduce Δr_h upon adsorption of HSA. To explain this reduction, we may consider two scenarios. First, we can hypothesize that the PEG layer remains unchanged upon protein adsorption, so proteins cannot penetrate. Based on this assumption, more protein molecules (as given by N_{max}) would adsorb onto the non-PEGylated than the PEGylated NPs. This is also reflected in the normalized numbers, $N_{max} / 4\pi r_h^2(0)^{(fit)}$, in which the surface density of HSA under saturation condition is less than half than for PEGylated *versus* non-PEGylated NPs. One thus could state that the degree of adsorption of HSA molecules onto PEGylated NPs is only 50% (with the number of adsorbed HSA molecules normalized to the surface area, $N_{max} / 4\pi r_h^2(0)^{(fit)}$) of the value observed for non-PEGylated NPs. Upon PEGylation, the thickness of the protein corona (Δr_h) also would be only around 50% of the one around non-PEGylated NPs. However, data obtained with PEGylated flat surfaces suggest that a second scenario may also be plausible. Proteins are known to be attracted to PEG layers by short-range forces[61]. If they are sufficiently small, they may penetrate the PEG layer and get trapped inside the polymer layer[62]. Larger proteins, by contrast, may interact with the outer part of the PEG layer and compress it[63]. Under this assumption, there could be a similar amount of proteins adsorbed to the non-PEGylated *versus* the PEGylated NPs. In the case of PEGylated NPs, however, there would be a reduced increase in Δr_h, as HSA has partly penetrated the PEG layer and, possibly, even compressed the PEG layer.

Structural information, *i.e.*, knowledge about the geometry of the PEG layer after HSA adsorption, is required to resolve these issues experimentally. In the case of flat surfaces, the thickness of PEG layers has been determined with X-ray photoelectron spectroscopy (XPS), ellipsometry[27], and atomic force microscopy (AFM)[64]. Direct structural information about the location of proteins has been obtained with reflectometric interference spectroscopy (RIfS) and neutron reflectometry[65]. The reflectrometry studies revealed that proteins can only penetrate into PEG layers of low grafting density. In this work, however, we are dealing with NP, *i.e.*, strongly curved surfaces, to which the above mentioned techniques are difficult to apply. We were thus not able to quantitatively determine the geometry of the PEG layer on the NP surface. The key parameter of interest would be the grafting density of PEG, *i.e.*, the number of PEG molecules *per* NP surface area. Depending on the grafting density, PEG layers are known to have different geometry, changing from a mushroom-like structure to a brush-like structure at higher grafting density.[66,67] Taking into account the reaction conditions, *i.e.*, the concentration of PEG during the attachment to the NP

surface, we estimate that the PEG molecules are non-densely adsorbed in mushroom conformation (*cf.* Supporting Information for detailed calculations). Our FCS data permit a precise determination of Δr_h, but yield no other structural information. The gel electrophoresis data (shown in Supporting Information) indicate that, under our experimental conditions, no more PEG can be added to the NPs, *i.e.*, the NP surface is saturated with PEG. However, also these data do not provide detailed structural information. Furthermore, also the dense appearance of the PEG layers in TEM images using negative staining (*cf.* Figure 1) is not suitable to obtain quantitative structural information.

To further address the key questions, whether protein adsorption changes the PEG conformation on our NPs, and where the proteins are located upon adsorption, we employed fluorescence lifetime measurements and quenching experiments. Optical properties of fluorophores are sensitive to their physicochemical environment. Solvatochromism is one such example, where a shift in the absorption and emission peaks occurs in response to a change in fluorophore environment[68]. Medium conditions, however, may also affect the fluorescence lifetime[69,70]. We observed that adsorption of HSA onto the polymer shell of NPs increases the fluorescence lifetime of the integrated fluorophore DY-636 (*cf.* Supporting Information for data). If the PEG shell around the polymer-coated NPs is so dense that HSA molecules cannot penetrate the PEG layer, they would not reach the underlying polymer-coating. Thus, the adsorption of HSA should not affect the lifetime of DY-636 in the polymer shell. However, we have observed a significant fluorescence lifetime increase of the DY-636 dye molecules in the polymer shell upon HSA binding that was similar for PEGylated and non-PEGylated NPs. This result supports our view that HSA molecules enter the PEG layer and bind to the negatively charged polymer surface (for a full discussion of these data, we refer to the Supporting Information). Additional experiments using potassium iodide as a fluorescence quencher lend additional support to this claim (*cf.* Supporting Information). Thus, although we cannot provide direct structural evidence, our fluorescence spectroscopy data strongly suggest that HSA at least partly penetrates the PEG layer, which would explain the reduced increase of Δr_h upon NP incubation with HSA. In this scenario, HSA molecules reside within the PEG coating of the NP rather than on the NP surface.

In order to assess the biological activity of PEG present on the surface of our NPs, we investigated the effect of the different coatings (PEG, glucose) on the internalization of NPs by cultured cells from the NIH/3T3 murine fibroblast cell line (ATCC, #CRL-1658). 3T3 cells were incubated for 12 h (37 °C, 5% CO_2) with Dulbecco´s modified Eagle´s medium (DMEM) supplemented with 10% fetal bovine serum and containing NPs at 5 or 10 nM concentrations (for details, *cf.* Supporting Information). Note, that serum-containing culture-conditions will cause the formation of a protein corona around the

NPs, which reduces NP uptake by cells as compared to serum-free culture conditions[50]. Then, the nuclei were fixed and stained in blue with 4',6-diamidino-2-phenylindole (DAPI) and the cell membrane in green with wheat germ agglutinin (WGA)-Alexa 488. Images of the cells were recorded by using confocal microscopy. Besides the blue (DAPI) and green (WGA-Alexa 488) fluorescence channels, we also recorded red fluorescence originating from the DY-636-labeled polymer coating around the NPs. With custom-made software written in Matlab (Mathworks), individual cells were automatically identified and masked, based on the nuclei/membrane staining as described in Supporting Information. Algorithms for cell detection and segmentation were provided by the open source software CellProfiler[71]. Then, the mean fluorescence intensity originating from NP emission within each cell mask (*i.e.*, the mean signal of all pixels corresponding to NPs inside one single cell) was determined and multiplied by the area of the cell. In this way, the integrated fluorescence I of each cell (= mean pixel intensity within the cell × cross section area of the cell) was determined, *cf.* Figure 3. The obtained value can be taken as proportional to the total uptake of NPs per cell because the height of the imaged plane relative to the growth surface was kept constant (*cf.* Supporting Information). The results are presented as average integrated fluorescence per cell. NPs adhering to the outer plasma membrane may contribute to the overall signal; however, we removed these NPs as thoroughly as possible by extensive washing before imaging. The fluorescence of non-internalized particles attached to the outer plasma membrane is negligible, as judged from inspection of the collected images (*cf.* Supporting Information).

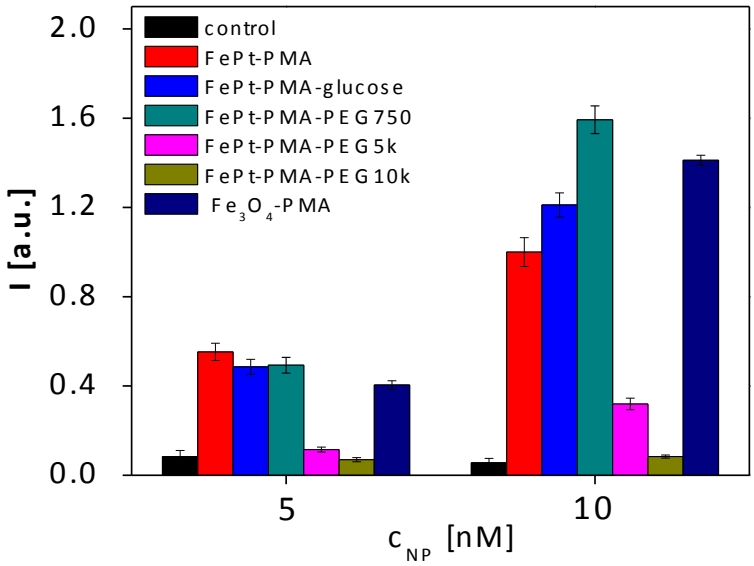

Figure 3: Integrated NP fluorescence *I* per cell (mean value ± standard deviation, obtained from 150 – 500 cells) after having incubated 3T3 fibroblasts in serum containing medium with NPs at concentrations c_{NP} = 5 nM or 10 nM. The intensity of Fe_3O_4 NPs was scaled with the ratio *R* (0.67) of the fluorescence per FePt NP to the

fluorescence per Fe_3O_4 NP. The control sample refers to the residual fluorescence of 3T3 cells without added NPs.

Because the fluorescent dyes were incorporated in the PMA polymer shell around the FePt core prior to further modification by PEG and glucose, these samples can be compared based on the fluorescence intensity in the cell samples. Also, FCS measurements verified that NP brightness did not change upon PEGylation. For the Fe_3O_4 NPs, however, the core and thus the amount of PMA shell is larger, and so is the number of fluorophores per NP. To normalize the fluorescence such that the signal reflects the number of NPs regardless of the size, the fluorescence intensity, *I*, of the Fe_3O_4 NPs was scaled with the ratio *R* of the fluorescence per FePt NP to the fluorescence per Fe_3O_4 NP ($R = I_{FePt}/I_{Fe3O4}$). This scaling factor was determined either by measuring the fluorescence intensity of solutions of PMA-coated FePt and Fe_3O_4 NPs with equal concentrations (R = 0.67, *cf.* the Supporting Information), or by assuming that the number of fluorophores scales with the surface area of the PMA-coating, as reported in Table 2: $R = r_h^2(0)^{(fit)}$ (FePt-PMA) / $r_h^2(0)^{(fit)}$ (Fe_3O_4-PMA) = $(5.4\ nm)^2/(6.7\ nm)^2 \approx 0.64$. The intensity data of incorporated Fe_3O_4 NPs were then multiplied by the scaling factor R = 0.67 for comparison with the intensity data of FePt NPs, as shown in Figure 3. NP uptake depends on the NP size; typically, bigger NPs are incorporated to a lesser extent. For citric acid stabilized NPs, for example, it has been shown that the number of NPs incorporated by the cells is reduced with increasing size (for diameters > 50 nm)[45]. However, in our case, the difference in $r_h(0)$ between the NP samples is too small in relation to the experimental uncertainty to afford a definitive statement about the size dependence of cellular uptake. For glucose modified NPs, we did not observe a reduction of uptake, although previous work (using a different cell line) has shown that functionalization of NPs with glucose can modify their uptake efficiency[72]. More specifically, glucose-functionalized NPs have been reported to be internalized into cells by lipid raft pathways instead of conventional clathrin-mediated endocytosis[73].

Cellular uptake is greatly reduced for our PEGylated FePt-PMA-PEG5k and –PEG10k NPs, whereas this trend is not observed or even inverted for FePt-PMA-PEG750 (*i.e.*, at 10 nM, the NP uptake was increased compared to the non-PEGylated NPs). Clearly, the effect is more pronounced for NPs covered with PEG of high M_W, in agreement with the literature[2,5,74]. While we cannot explain the increase in uptake of FePt-PMA-PEG750 as compared to FePt-PMA at 10 nM NP concentration, uptake of NPs covered with 10 kDa PEG (FePt-PMA-10 kDa PEG) is largely reduced to an amount as low as *ca.* 10% of the value for non-PEGylated NPs (FePt-PMA), *cf.* Figure 3. Uptake suppression is not due to the increased size upon PEGylation because the larger Fe_3O_4 control sample was incorporated to a greater degree. Thus, uptake reduction of PEGylated NPs is specific for the high molecular weight PEG coating.

Conclusions

We have presented a systematic investigation of protein adsorption onto PEGylated, polymer-coated NPs. In this study, we have also included control NPs without PEG coating but with modified size and surface charge to prove that the observed effects result from the unique interaction properties of PEGylated surfaces rather than mere changes of NP size and surface charge. Even though the PEGs were grafted onto the NPs at high density, this was clearly not sufficient to completely abolish protein adsorption. In fact, the small size of the NPs, giving rise to a strong surface curvature, for obvious geometric reasons, requires an even denser surface grafting than for planar surfaces so as to efficiently prevent protein penetration into the PEG layer.

Of note, the micromolar affinities of HSA adsorption reported here indicate that proteins form a rather weakly bound, or soft corona around the NPs. Consequently, it is not possible to directly quantify the amount of adsorbed HSA *in situ* by commonly used techniques such as mass spectroscopy or gel electrophoresis because purification from unbound protein would disturb the dynamic equilibrium between free and NP-bound HSA proteins. Unlike most other approaches, the FCS method used here permits *in situ* measurements in thermal equilibrium.

Upon HSA binding, non-PEGylated NPs (FePt-PMA, FePt-PMA-glucose, Fe_3O_4-PMA) displayed a radius increase of ~3 nm at saturation, which is consistent with formation of a monolayer of HSA on top of the NP surfaces, with the HSA molecules adsorbing with one of their triangular faces[49]. Of note, this size increase has been observed for chemically different, small NPs as well.[75] In contrast, the size increase resulting from HSA adsorption was significantly reduced to ~1.5 nm for our PEGylated NPs. This difference could, in principle, result from smaller numbers of binding sites for HSA molecules on top of the PEG layers enshrouding the NPs. However, we have gathered spectroscopic evidence, by using fluorescence lifetime analysis and quenching studies (with KI) of the DY-626 fluorophores attached to the NPs, strongly suggesting that HSA penetrates the PEG layer of our NPs and resides within the PEG layer. Presumably, they are adsorbed to the underlying surface to which the PEG chains are grafted. This result is in line with previous studies carried out on planar PEG layers, examining protein adsorption as a function of the grafting density and chain length of the PEG molecules forming the layer[14,25,27].

In agreement with previous studies, we have observed that PEGylation reduces NP uptake by cultured cells[1,2,4,5,7,10,11,13]. Whereas proteins were adsorbed onto the outer surface of the non-PEGylated NPs, proteins are buried inside the PEG layer for PEGylated NPs, so that the protein corona is hidden from the interface, and the NPs

continue to interact with cells *via* their PEG surfaces, even though proteins are adsorbed.

In regard to the future development of NPs surface coatings, we stress that PEGylation may not always be the optimal strategy when developing devices for targeted drug delivery. Notably, for drug targeting *via* intravenous delivery, the two key consequences of PEGylation, namely reduced cellular uptake and increased retention times, are conflicting. Long retention times in the body are highly desirable to obtain longer circulation of the NPs in the blood vessels, thus offering a higher chance to reach, *e.g.*, a tumor site by passive targeting *via* the enhanced permeation and retention (EPR) effect. However, poor NP uptake by cells inside tumor tissue due to PEGylation is not desirable[76,77]. Zwitterionic surfaces are presently discussed as promising alternatives[78-83], ensuring extended retention times as well as enhanced NP internalization by cells. Thus, detailed studies of interactions of such NPs with proteins will be highly desirable for the future.

Acknowledgments:

BP acknowledges the Alexander von Humboldt Foundation for a postdoctoral fellowship. This work was supported by the Deutsche Forschungsgemeinschaft (GRK 1782, grant to WJP), the European Research Council (Starting Grant 239931-NANOPUZZLE to JMdlF), and the KIT in the context of the Helmholtz STN Program (to GUN). The authors are grateful to Karsten Kantner for determining NP concentrations by ICP-MS.

References:

1. Zhang, Y.; Kohler, N.; Zhang, M. Q., Surface modification of superparamagnetic magnetite nanoparticles and their intracellular uptake. *Biomaterials* **2002**, 23, 1553-1561.
2. Xie, J.; Xu, C.; Kohler, N.; Hou, Y.; Sun, S., Controlled PEGylation of Monodisperse Fe3O4 Nanoparticles for Reduced Non-Specific Uptake by Macrophage Cells. *Adv. Mater.* **2007**, 19, 3163-3166.
3. Ryman-Rasmussen, J. P.; Riviere, J. E.; Monteiro-Riviere, N. A., Variables Influencing Interactions of Untargeted Quantum Dot Nanoparticles with Skin Cells and Identification of Biochemical Modulators. *Nano Lett.* **2007**, 7, 1344-1348.
4. Hak, S.; Helgesen, E.; Hektoen, H. H.; Huuse, E. M.; Jarzyna, P. A.; Mulder, W. J. M.; Haraldseth, O.; Davies, C. d. L., The Effect of Nanoparticle Polyethylene Glycol Surface Density on Ligand-Directed Tumor Targeting Studied in Vivo by Dual Modality Imaging. *ACS Nano* **2012**, 6, 5648.
5. Gref, R.; Lück, M.; Quellec, P.; Marchand, M.; Dellacherie, E.; Harnisch, S.; Blunk, T.; Müller, R. H., 'Stealth' Corona-Core Nanoparticles Surface Modified by Polyethylene Glycol (PEG): Influences of the Corona (PEG Chain Length and Surface Density) and of the Core

Composition on Phagocytic Uptake and Plasma Protein Adsorption. *Colloids and Surfaces B* **2000**, 18, 301-313.
6. He, Q.; Zhang, J.; Shi, J.; Zhu, Z.; Zhang, L.; Bu, W.; Guo, L.; chen, Y., The effect of PEGylation of mesoporous silica nanoparticles on nonspecific binding of serum proteins and cellular responses. *Biomaterials* **2010**, 31, 1085-1092.
7. Dai, Q.; Walkey, C.; Chan, W. C., Polyethylene Glycol Backfilling Mitigates the Negative Impact of the Protein Corona on Nanoparticle Cell Targeting. *Angew Chem Int Ed Engl* **2014**.
8. Ballou, B.; Lagerholm, B. C.; Ernst, L. A.; Bruchez, M. P.; Waggoner, A. S., Noninvasive Imaging of Quantum Dots in Mice. *Bioconjugate Chem.* **2004**, 15, 79-86.
9. Daou, T. J.; Li, L.; Reiss, P.; Josserand, V.; Texier, I., Effect of Poly(ethylene glycol) Length on the in Vivo Behavior of Coated Quantum Dots. *Langmuir* **2009**, 25, 3040-3044.
10. Lipka, M.; Semmler-Behnke, M.; Sperling, R. A.; Wenk, A.; Takenaka, S.; Schleh, C.; Kissel, T.; Parak, W. J.; Kreyling, W. G., Biodistribution of PEG-modified gold nanoparticles following intratracheal instillation and intravenous injection. *Biomaterials* **2010**, 31, 6574-6581.
11. von Maltzahn, G.; Park, J.-H.; Agrawal, A.; Bandaru, N. K.; Das, S. K.; Sailor, M. J.; Bhatia, S. N., Computationally Guided Photothermal Tumor Therapy Using Long-Circulating Gold Nanorod Antennas. *Cancer Res.* **2009**, 69, 3892-3900.
12. Cho, W. S.; Cho, M.; Jeong, J.; Choi, M.; Han, B. S.; Shin, H. S.; Hong, J.; Chung, B. H.; Jeong, J.; Cho, M. H., Size-dependent tissue kinetics of PEG-coated gold nanoparticles. *Toxicol. Appl. Pharmacol.* **2010**, 245, 116-23.
13. Perrault, S. D.; Walkey, C.; Jennings, T.; Fischer, H. C.; Chan, W. C. W., Mediating Tumor Targeting Efficiency of Nanoparticles Through Design. *Nano Lett.* **2009**, 9, 1909-1915.
14. Kingshott, P.; Thissen, H.; Griesser, H. J., Effects of cloud-point grafting, chain length, and density of PEG layers on competitive adsorption of ocular proteins. *Biomaterials* **2002**, 23, 2043-2056.
15. Pasche, S.; De Paul, S. M.; Voros, J.; Spencer, N. D.; Textor, M., Poly(L-lysine)-graft-poly(ethylene glycol) assembled monolayers on niobium oxide surfaces: A quantitative study of the influence of polymer interfacial architecture on resistance to protein adsorption by ToF-SIMS and in situ OWLS. *Langmuir* **2003**, 19, 9216-9225.
16. Moros, M.; Pelaz, B.; Lopez-Larrubia, P.; Garcia-Martin, M. L.; Grazu, V.; de la Fuente, J. M., Engineering biofunctional magnetic nanoparticles for biotechnological applications. *Nanoscale* **2010**, 2, 1746-1755.
17. Gordon, D. L.; Rice, J. L., Opsonin-dependent and independent surface phagocytosis of S. aureus proceeds independently of complement and complement receptors. *Immunology* **1988**, 64, 709-714.
18. Treuel, L.; Brandholt, S.; Maffre, P.; Wiegele, S.; Shang, L.; Nienhaus, G. U., Impact of Protein Modification on the Protein Corona on Nanoparticles and Nanoparticle Cell Interactions. *ACS Nano* **2014**, - 8, 503 - 513.
19. McPherson, T.; Kidane, A.; Szleifer, I.; Park, K., Prevention of Protein Adsorption by Tethered Poly(ethylene oxide) Layers: Experiments and Single-Chain Mean-Field Analysis. *Langmuir* **1998**, 14, 176-186.
20. Michel, R.; Pasche, S.; Textor, M.; Castner, D. G., Influence of PEG Architecture on Protein Adsorption and Conformation. *Langmuir* **2005**, 21, 12327-12332.
21. Pasche, S.; Vörös, J.; Griesser, H. J.; Spencer, N. D.; Textor, M., Effects of Ionic Strength and Surface Charge on Protein Adsorption at PEGylated Surfaces. *The Journal of Physical Chemistry B* **2005**, 109, 17545-17552.
22. Mrksich, M.; Whitesides, G. M., Using self-assembled monolayers to understand the interactions of man-made surfaces with proteins and cells. *Annu. Rev. Biophys. Biomol. Struct.* **1996**, 25, 55-78.

23. Ostuni, E.; Chapman, R. G.; Holmlin, R. E.; Takayama, S.; Whitesides, G. M., A Survey of Structure−Property Relationships of Surfaces that Resist the Adsorption of Protein. *Langmuir* **2001**, 17, 5605-5620.
24. Mrksich, M.; Chen, C. S.; Xia, Y.; Dike, L. E.; Ingber, D. E.; Whitesides, G. M., Controlling cell attachment on contoured surfaces with self-assembled monolayers of alkanethiolates on gold. *Proc. Natl. Acad. Sci. U. S. A.* **1996**, 93, 10775-8.
25. Zhang, M.; Desai, T.; Ferrari, M., Proteins and cells on PEG immobilized silicon surfaces. *Biomaterials* **1998**, 19, 953-960.
26. Jeon, S. I.; Lee, J. H.; Andrade, J. D.; De Gennes, P. G., Protein—surface interactions in the presence of polyethylene oxide: I. Simplified theory. *J. Colloid Interface Sci.* **1991**, 142, 149-158.
27. Sofia, S. J.; Premnath, V.; Merrill, E. W., Poly(ethylene oxide) grafted to silicon surfaces: Grafting density and protein adsorption. *Macromolecules* **1998**, 31, 5059-5070.
28. Piehler, J.; Brecht, A.; Valiokas, R.; Liedberg, B.; Gauglitz, G., A high-density poly(ethylene glycol) polymer brush for immobilization on

glass-type surfaces. *Biosensors and Bioelectronics* **2000**, 15, 473-483.
29. Sheth, S. R.; Leckband, D., Measurements of attractive forces between proteins and end-grafted poly(ethylene glycol) chains. *Proc. Natl. Acad. Sci. U. S. A.* **1997**, 94, 8399-8404.
30. Klapper, Y.; Vranceanu, M.; Ishitsuka, Y.; Evans, D.; Scheider, D.; Nienhaus, G. U.; Leneweit, G., Surface energy of phospholipid bilayers and the correlation to their hydration. *J. Colloid Interface Sci.* **2013**, 390, 267-274.
31. Yang, Z.; Galloway, J. A.; Yu, H., Protein Interactions with Poly(ethylene glycol) Self-Assembled Monolayers on Glass Substrates: Diffusion and Adsorption. *Langmuir* **1999**, 15, 8405-8411.
32. Heyes, C. D.; Kobitski, A. Y.; Amirgoulova, E. V.; Nienhaus, G. U., Biocompatible surfaces for specific tethering of individual protein molecules. *J. Phys. Chem. B* **2004**, 108, 13387-13394.
33. Amirgoulova, E. V.; Groll, J.; Heyes, C. D.; Ameringer, T.; Rocker, C.; Moller, M.; Nienhaus, G. U., Biofunctionalized polymer surfaces exhibiting minimal interaction towards immobilized proteins. *ChemPhysChem* **2004**, 5, 552-555.
34. Groll, J.; Amirgoulova, E. V.; Ameringer, T.; Heyes, C. D.; Rocker, C.; Nienhaus, G. U.; Moller, M., Biofunctionalized, ultrathin coatings of cross-linked star-shaped poly(ethylene oxide) allow reversible folding of immobilized proteins. *J. Am. Chem. Soc.* **2004**, 126, 4234-4239.
35. Heyes, C. D.; Groll, J.; Moller, M.; Nienhaus, G. U., Synthesis, patterning and applications of star-shaped poly(ethylene glycol) biofunctionalized surfaces. *Mol. BioSyst.* **2007**, 3, 419-430.
36. Harder, P.; Grunze, M.; Dahint, R.; Whitesides, G. M.; Laibinis, P. E., Molecular Conformation in Oligo(ethylene glycol)-Terminated Self-Assembled Monolayers on Gold and Silver Surfaces Determines Their Ability To Resist Protein Adsorption. *The Journal of Physical Chemistry B* **1998**, 102, 426-436.
37. Wang, R. L. C.; Kreuzer, H. J.; Grunze, M., Molecular Conformation and Solvation of Oligo(ethylene glycol)-Terminated Self-Assembled Monolayers and Their Resistance to Protein Adsorption. *The Journal of Physical Chemistry B* **1997**, 101, 9767-9773.
38. Sperling, R. A.; Pellegrino, T.; Li, J. K.; Chang, W. H.; Parak, W. J., Electrophoretic Separation of Nanoparticles with a Discrete Number of Functional Groups. *Adv. Funct. Mater.* **2006**, 16, 943-948.
39. Sperling, R. A.; Liedl, T.; Duhr, S.; Kudera, S.; Zanella, M.; Lin, C.-A. J.; Chang, W. H.; Braun, D.; Parak, W. J., Size Determination of (Bio-) Conjugated Water-Soluble Colloidal Nanoparticles: A Comparison of Different Techniques. *J. Phys. Chem. C* **2007**, 111, 11552-11559.

40. Parak, W. J.; Pellegrino, T.; Micheel, C. M.; Gerion, D.; Williams, S. C.; Alivisatos, A. P., Conformation of oligonucleotides attached to gold nanocrystals probed by gel electrophoresis. *Nanoletters* **2003**, 3, 33-36.
41. Pellegrino, T.; Sperling, R. A.; Alivisatos, A. P.; Parak, W. J., Gelelectrophoresis of Gold-DNA Nanoconjugates. *J. Biomed. Biotechnol.* **2007**, Article ID 26796, 1-9.
42. Brandenberger, C.; Mühlfeld, C.; Ali, Z.; Lenz, A.-G.; Schmid, O.; Parak, W. J.; Gehr, P.; Rothen-Rutishauser, B., Quantitative Evaluation of Cellular Uptake and Trafficking of Plain and Polyethylene Glycol-Coated Gold Nanoparticles. *Small* **2010**, 6, 1669-1678
43. Van_Hoecke, K.; De Schamphelaer, K. A. C.; Ali, Z.; Zhang , F.; Elsaesser, A.; Rivera_Gil, P.; Parak , W. J.; Smagghe, G.; Janssen, C. R., Ecotoxicity and uptake of polymer coated gold nanoparticles. *Nanotoxicology* **2013**, 7, 37-47.
44. Rivera Gil, P.; Jimenez de Aberasturi, D.; Wulf, V.; Pelaz, B.; del Pino, P.; Zhao, Y.; de la Fuente, J.; Ruiz de Larramendi, I.; Rojo, T.; Liang, X.-J.; Parak, W. J., The Challenge to Relate the Physicochemical Properties of Colloidal Nanoparticles to Their Cytotoxicity. *Acc. Chem. Res.* **2013**, 46, 743-749.
45. Chithrani, B. D.; Ghazan, A. A.; Chan, C. W., Determining the Size and the Shape dependence of gold nanoparticle uptake into mammalian cells. *Nano Lett.* **2006**, 6, 662-668.
46. Pellegrino, T.; Kudera, S.; Liedl, T.; Javier, A. M.; Manna, L.; Parak, W. J., On the Development of Colloidal Nanoparticles towards Multifunctional Structures and their Possible Use for Biological Applications. *Small* **2005**, 1, 48-63.
47. Nazarenus, M.; Zhang, Q.; Soliman, M. G.; del Pino, P.; Pelaz, B.; Carregal_Romero, S.; Rejman, J.; Rothen-Ruthishauser, B.; Clift, M. J. D.; Zellner, R.; Nienhaus, G. U.; Delehanty, J. B.; Medintz, I. L.; Parak, W. J., In vitro Interaction of Colloidal Nanoparticles with Mammalian Cells: What Have We Learned Thus Far? *Beilstein J. Nanotechnol.* **2014**, 5, 1477-1490.
48. Zhang, F.; Lees, E.; Amin, F.; Rivera_Gil, P.; Yang, F.; Mulvaney, P.; Parak, W. J., Polymer-Coated Nanoparticles: A Universal Tool for Biolabelling Experiments. *Small* **2011**, 7, 3113-3127.
49. Röcker, C.; Pötzl, M.; Zhang, F.; Parak, W. J.; Nienhaus, G. U., A Quantitative Fluorescence Study of Protein Monolayer Formation on Colloidal Nanoparticles. *Nat. Nanotechnol.* **2009**, 4, 577-580.
50. Jiang, X.; Weise, S.; Hafner, M.; Röcker, C.; Zhang, F.; Parak, W. J.; Nienhaus, G. U., Quantitative Analysis of the Protein Corona on FePt Nanoparticles Formed by Transferrin Binding. *J. R. Soc., Interface* **2010**, 7, S5-S13.
51. Maffre, P.; Nienhaus, K.; Amin, F.; Parak, W. J.; Nienhaus, G. U., Characterization of Protein Adsorption onto FePt Nanoparticles Using Dual-Focus Fluorescence Correlation Spectroscopy. *Beilstein J. Nanotechnol.* **2011**, 2, 374–383.
52. Nienhaus, G. U.; Maffre, P.; Nienhaus, K., Studying the protein corona on nanoparticles by FCS. *Methods Enzymol.* **2013**, 519, 115-137.
53. Fernández-Argüelles, M. T.; Yakovlev, A.; Sperling, R. A.; Luccardini, C.; Gaillard, S.; Medel, A. S.; Mallet, J.-M.; Brochon, J.-C.; Feltz, A.; Oheim, M.; Parak, W. J., Synthesis and Characterization of Polymer-Coated Quantum Dots with Integrated Acceptor Dyes as FRET-based Nanoprobes. *Nano Lett.* **2007**, 7, 2613-2617.
54. Cui, M.; Liu, R.; Deng, Z.; Ge, G.; Liu, Y.; Xie, L., Quantitative study of protein coronas on gold nanoparticles with different surface modifications. *Nano Res.* **2014**, 7.
55. Schweiger, C.; Hartmann, R.; Zhang, F.; Parak, W. J.; Kissel, T.; Rivera Gil, P., Quantification of the Internalization Patterns of Superparamagnetic Iron Oxide Nanoparticles with Opposite Charge. *J. Nanobiotechnol.* **2012**, 10, 28.
56. Hühn, D.; Kantner, K.; Geidel, C.; Brandholt, S.; De Cock, I.; Soenen, S. J. H.; Rivera Gil, P.; Montenegro, J.-M.; Braeckmans, K.; Müllen, K.; Nienhaus , G. U.; Klapper, M.; Parak, W. J., Polymer-Coated Nanoparticles Interacting with Proteins and Cells: Focusing on the Sign of the Net Charge. *ACS Nano* **2013**, 7, 3253-3263.

57. Caballero-Díaz, E.; Pfeiffer, C.; Kastl, L.; Rivera-Gil, P.; Simonet, B.; Valcárcel, M.; Jiménez-Lamana, J.; Laborda, F.; Parak, W. J., The Toxicity of Silver Nanoparticles Depends on Their Uptake by Cells and Thus on Their Surface Chemistry. *Part. Part. Syst. Charact.* **2013**, 30, 1079-1085.
58. del_Pino, P.; Pelaz, B.; Zhang, Q.; Maffre, P.; Nienhaus, G. U.; Parak, W. J., Protein corona formation around nanoparticles-from the past to the future. *Materials Horizons* **2014**, 1, 301-313.
59. Huang, R.; Carney, R. P.; Ikuma, K.; Stellacci, F.; Lau, B. L. T., Effects of Surface Compositional and Structural Heterogeneity on Nanoparticle–Protein Interactions: Different Protein Configurations. *ACS Nano* **2014**, 8, 5402-5412.
60. Dominguez-Medina, S.; McDonough, S.; Swanglap, P.; Landes, C. F.; Link, S., In Situ Measurement of Bovine Serum Albumin Interaction with Gold Nanospheres. *Langmuir* **2012**, 28, 9131-9139.
61. Halperin, A., Polymer brushes that resist adsorption of model proteins: Design parameters. *Langmuir* **1999**, 15, 2525-2533.
62. Gon, S.; Santore, M. M., Sensitivity of Protein Adsorption to Architectural Variations in a Protein-Resistant Polymer Brush Containing Engineered Nanoscale Adhesive Sites. *Langmuir* **2011**, 27, 15083-15091.
63. Gon, S.; Bendersky, M.; Ross, J. L.; Santore, M. M., Manipulating Protein Adsorption using a Patchy Protein-Resistant Brush. *Langmuir* **2010**, 26, 12147-12154.
64. Park, H.-W.; Choi, J.; Ohn, K.; Lee, H.; Kim, J. W.; Won, Y.-Y., Study of the Air–Water Interfacial Properties of Biodegradable Polyesters and Their Block Copolymers with Poly(ethylene glycol). *Langmuir* **2012**, 28, 11555-11566.
65. Schneck, E.; Schollier, A.; Halperin, A.; Moulin, M.; Haertlein, M.; Sferrazza, M.; Fragneto, G., Neutron Reflectometry Elucidates Density Profiles of Deuterated Proteins Adsorbed onto Surfaces Displaying Poly(ethylene glycol) Brushes: Evidence for Primary Adsorption. *Langmuir* **2013**, 29, 14178-14187.
66. Backmann, N.; Kappeler, N.; Braun, T.; Huber, F.; Lang, H.-P.; Gerber, C.; Lim, R. Y. H., Sensing surface PEGylation with microcantilevers. *Beilstein J. Nanotechnol.* **2010**, 1, 3-13.
67. Perry, J. L.; Reuter, K. G.; Kai, M. P.; Herlihy, K. P.; Jones, S. W.; Luft, J. C.; Napier, M.; Bear, J. E.; DeSimone, J. M., PEGylated PRINT Nanoparticles: The Impact of PEG Density on Protein Binding, Macrophage Association, Biodistribution, and Pharmacokinetics. *Nano Lett.* **2012**, 12, 5304-5310.
68. Amin, F.; Yushchenko, D. A.; Montenegro, J. M.; Parak, W. J., Integration of Organic Fluorophores in the Surface of Polymer-Coated Colloidal Nanoparticles for Sensing the Local Polarity of the Environment. *ChemPhysChem* **2012**, 13, 1030-1035.
69. Choi, J. Y.; Park, E. J.; Chang, S. H.; Kang, T. J., Solvent Effects on the Solvatochromism of 7-Aminocoumarin Derivatives in Neat and Binary Solvent Mixtures: Correlation of the Electronic Transition Energies with the Solvent Polarity Parameters. *Bull. Korean Chem. Soc.* **2009**, 30, 1452-1458.
70. Berezin, M. Y.; Lee, H.; Akers, W.; Achilefu, S., Near Infrared Dyes as Lifetime Solvatochromic Probes for Micropolarity Measurements of Biological Systems. *Biophys. J.* **2007**, 93, 2892-2899.
71. Carpenter, A.; Jones, T.; Lamprecht, M.; Clarke, C.; Kang, I.; Friman, O.; Guertin, D.; Chang, J.; Lindquist, R.; Moffat, J.; Golland, P.; Sabatini, D., CellProfiler: image analysis software for identifying and quantifying cell phenotypes. *Genome Biology* **2006**, 7, R100.
72. De la Fuente, J. M.; Alcantara, D.; Penades, S., Cell Response to Magnetic Glyconanoparticles: Does the Carbohydrate Matter? *NanoBioscience, IEEE Transactions on* **2007**, 6, 275-281.
73. Moros, M.; Hernáez, B.; Garet, E.; Dias, J. T.; Sáez, B.; Grazú, V.; González-Fernández, Á.; Alonso, C.; Fuente, J. M. d. l., Monosaccharides versus PEG-Functionalized NPs: Influence in the Cellular Uptake. *ACS Nano* **2012**, 6, 1565-1577.

74. Harakeh, S.; Abdel-Massih, R. M.; Rivera_Gil, P.; Sperling, R. A.; Meinhardt, A.; Niedwiecki, A.; Rath, M.; Parak, W. J.; Baydoun, E., The effect of PEG-coated gold nanoparticles on the anti-proliferative potential of Specific Nutrient Synergy. *Nanotoxicology* **2010**, 4, 177-185.
75. Maffre, P.; Brandholt, S.; Nienhaus, K.; Shang, L.; Parak, W. J.; Nienhaus, G. U., Effects of surface functionalization on the adsorption of human serum albumin onto nanoparticles a fluorescence correlation spectroscopy study. *Beilstein Journal of Nanotechnololgy* **2014**, 5, 2036 2047.
76. Zhang, G.; Yang, Z.; Lu, W.; Zhang, R.; Huang, Q.; Tian, M.; Li, L.; Liang, D.; Li, C., Influence of anchoring ligands and particle size on the colloidal stability and in vivo biodistribution of polyethylene glycol-coated gold nanoparticles in tumor-xenografted mice. *Biomaterials* **2009**, 30, 1928-1936.
77. Duan, X.; Li, Y., Physicochemical Characteristics of Nanoparticles Affect Circulation, Biodistribution, Cellular Internalization, and Trafficking. *Small* **2013**, 9, 1521-1532.
78. Zhou, W.; Shao, J.; Jin, Q.; Wei, Q.; Tang, J.; Ji, J., Zwitterionic phosphorylcholine as a better ligand for gold nanorods cell uptake and selective photothermal ablation of cancer cells. *Chem. Commun.* **2010**, 46, 1479-1481.
79. Murthy, A. K.; Stover, R. J.; Hardin, W. G.; Schramm, R.; Nie, G. D.; Gourisankar, S.; Truskett, T. M.; Sokolov, K. V.; Johnston, K. P., Charged Gold Nanoparticles with Essentially Zero Serum Protein Adsorption in Undiluted Fetal Bovine Serum. *J. Am. Chem. Soc.* **2013**, 135, 7799-7802.
80. Muro, E.; Pons, T.; Lequeux, N.; Fragola, A.; Sanson, N.; Lenkei, Z.; Dubertret, B., Small and stable sulfobetaine zwitterionic quantum dots for functional live-cell imaging. *J. Am. Chem. Soc.* **2010**, 132, 4556-7.
81. Wang, T.; Bai, J.; Jiang, X.; Nienhaus, G. U., Cellular uptake of nanoparticles by membrane penetration: a study combining confocal microscopy with FTIR spectroelectrochemistry. *ACS Nano* **2012**, 6, 1251-9.
82. Jiang, X.; Röcker, C.; Hafner, M.; Nienhaus, G. U., Endo- and Exocytosis of Zwitterionic Quantum Dot Nanoparticles by Living Cells. *ACS Nano* **2010**, 4, 6787-6797.
83. Breus, V. V.; Heyes, C. D.; Tron, K.; Nienhaus, G. U., Zwitterionic Biocompatible Quantum Dots for Wide pH Stability and Weak Nonspecific Binding to Cells. *ACS Nano* **2009**, 3, 2573-2580.